



NUMERICAL INVESTIGATIONS ON RECTANGULAR SQUAT REINFORCED CONCRETE WALLS UNDER BI-DIRECTIONAL LOADING

A. Niroomandi⁽¹⁾, M. Soleymani Ashtiani⁽²⁾, S. Pampanin⁽³⁾, R. P. Dhakal⁽⁴⁾,

⁽¹⁾ PhD candidate, University of Canterbury, arsalan.niroomandi@pg.canterbury.ac.nz

⁽²⁾ PhD, Structural Engineer, Ian Connor Consulting Ltd., ms.ashtiani81@gmail.com

⁽³⁾ Professor, University of Canterbury, stefano.pampanin@canterbury.ac.nz

⁽⁴⁾ Professor, University of Canterbury, rajesh.dhakal@canterbury.ac.nz

Abstract

In recent earthquakes in Chile and New Zealand (2010 and 2011, respectively), reinforced concrete (RC) walls underwent failure mechanisms which were not observed/reported in previous earthquakes. Some of these failure modes included out-of-plane displacements, which could potentially result from bi-directional excitations. As a result, a global concern has risen on the contribution of bi-directional loading towards performance and failure mechanisms of RC walls. Nevertheless the effects of bi-directional loading on design/assessment of rectangular walls have not yet been scrutinized. Squat RC walls are widely used as lateral load resisting system in different structures. Few investigations are carried out on seismic behaviour of such walls. There is still a significant uncertainty regarding the behaviour of these walls under earthquake loading as well as their failure mechanisms, and strengths and deformation capacities.

This paper presents results of a preliminary numerical investigation on the effect of bi-directional loading on rectangular squat RC walls. The numerical study is conducted using Finite Element (FE) analysis by DIANA. The FE model has been verified against experimental tests in another study. This preliminary parametric study is performed in order to identify the key parameters influencing seismic performance of rectangular squat RC walls under uni- and bi-directional loadings. Parameters such as confinement length, thickness, shear reinforcement and longitudinal reinforcement ratios are investigated in this study. The study also evaluates the effect of bi-directional loading on the stiffness, strength and drift capacity and failure modes of squat walls. More walls will be investigated for each parameter in a future study by the authors.

Keywords: rectangular squat RC walls; numerical parametric study; bi-directional loading; crack width; failure mode

1. Introduction

In recent earthquakes in Chile and New Zealand (2010 and 2011, respectively), peculiar failure mechanisms were observed in RC walls (Fig. 1) which differed from the traditional 2D-based response [1]. One of the researchers' concerns after these observations is the contribution of bi-directional loading to these failure modes.



Fig. 1 – Wall failure modes observed in recent earthquakes in (a) Chile [2] and (b) New Zealand [3]

Squat RC walls are widely used as lateral load resisting system in low-rise buildings. These are also used in high-rise structures when the base shear is high and the wall is only used over the first few stories [4]. Squat walls are defined as walls with height-to-length ratio less than 1.5 [5]. Few investigations are carried out on seismic behaviour of such walls [4, 6-9]. Typical failure modes of squat walls include diagonal tension, diagonal compression and sliding shear (Fig. 2). It is worth noting that such sliding displacements shown in Fig. 2c can lead to a significant reduction of stiffness and consequently a reduction of energy dissipation [4].

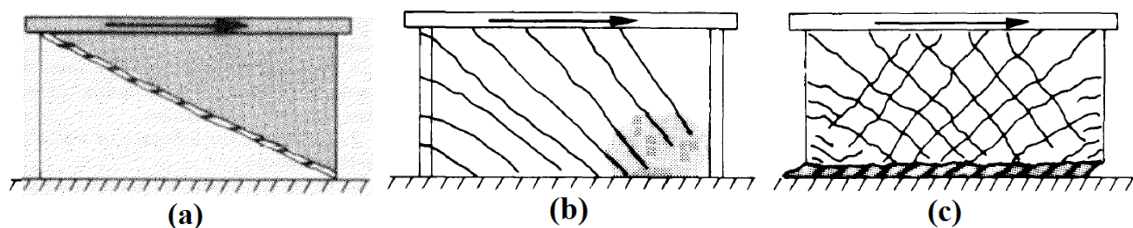


Fig. 2 – Typical squat walls failure modes (a) diagonal tension, (b) diagonal compression (c) sliding shear [4]

In this paper, a FE model (using DIANA) capable of simulating RC walls under uni- and bi-directional loadings is utilized to investigate squat walls under different loading regimes. The model has been validated against the experimental tests on walls under uni- and bi-directional loadings conducted by Kabeyasawa et al. [10] in a previous study by Niroomandi et al. [11]. The effects of parameters such as confinement length, thickness, longitudinal and shear reinforcement ratio on the performance of squat walls under uni- and bi-directional loadings are scrutinized in terms of force-displacement curves and failure modes.

2. Wall properties

A preliminary investigation has been conducted on squat walls using section analysis, while shear failure was controlled by the method shown in Fig. 3. Lateral force vs. displacement envelope (capacity curves) were calculated based on the modified UCSD method proposed by Krolicki et al. [12].

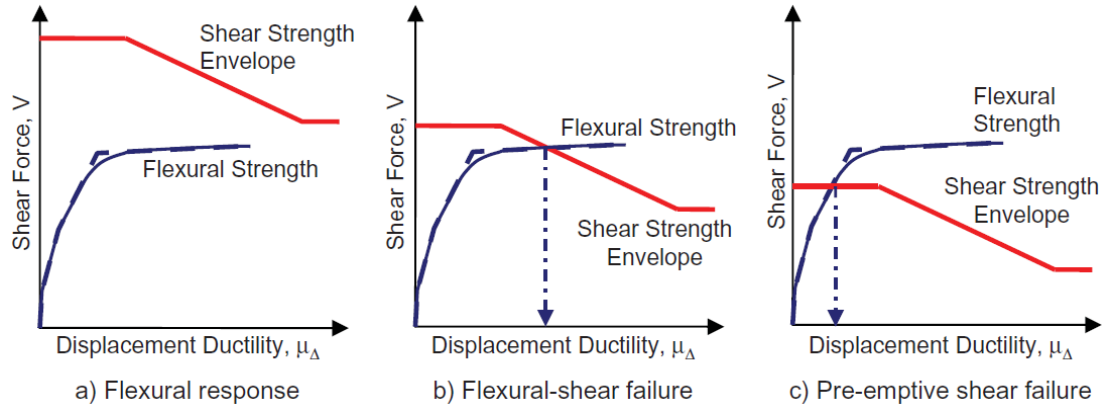


Fig. 3 – Considering shear failure in the section analysis [12]

It was found that confinement length, thickness, axial load ratio, longitudinal and shear reinforcement ratio are the most affecting parameters on the shear strength of squat walls. Since high axial load ratio is not common for squat walls [4] due to their geometric characteristics and use, the effect of high axial load ratio is not investigated in this study. However this parameter was investigated for a wall with a zero axial load. Based on the results of the section-analysis/shear-strength-envelope, the preliminary numerical study is conducted using the parameters shown in Table 1. Longitudinal reinforcements ratio are assigned to the boundary zones and web with respect to the minimum and maximum reinforcement ratio of the New Zealand code [13]. It should be noted that all walls are fully confined in the boundary zones to avoid flexural failure. The walls described in Table 1 were investigated under uni- and bi-directional loadings. Concrete and steel material properties are also tabulated in Table 2.

Table 1 – Walls characteristics

	Name	W-Bench	W-Confine	W-Thick	W-Long	W-shear	W-axial
Boundary Zone (BZ)	Cross section (mm)	370×250	670×250	350×150	370×250	370×250	370×250
	Longitudinal reinforcement ratio, $A_{s,BZ}/(l_w \times t)$	0.00375	0.004	0.00375	0.005625	0.00375	0.00375
	Transverse reinforcement ratio, $A_{sv}/(s \times t)$	0.006	0.006	0.006	0.006	0.006	0.006
Web	Length (mm)	2260	1660	2300	2260	2260	2260
	Thickness (mm)	250	250	150	250	250	250
	Longitudinal reinforcement ratio, $A_{s,web}/(l_w \times t)$	0.0025	0.002	0.0025	0.00375	0.0025	0.0025
	Shear reinforcement ratio, $A_{sv}/(h_w \times t)$	0.0014	0.0014	0.0014	0.0014	0	0.0014
Total longitudinal reinforcement ratio, $A_s/(l_w \times t)$		0.01	0.01	0.01	0.015	0.01	0.01
Axial load ratio, $P/(l_w \times t \times f_c)$		0.05	0.05	0.05	0.05	0.05	0
Shear span ratio, $M/(V \times l_w)$	In-plane direction	1	1	1	1	1	1
	Out-of-plane direction	0.5	0.5	0.5	0.5	0.5	0.5

Table 2 – Material properties

Concrete	Elastic Modulus (N/mm ²)	27386
	Compressive strength (N/mm ²)	30
	Tensile strength (N/mm ²)	1.7
Steel	Elastic Modulus (N/mm ²)	200000
	Yield strength (N/mm ²)	500
	Ultimate strength (N/mm ²)	650
	Ultimate strain (mm/mm)	0.06

The details of each wall are also shown in Fig. 4. In this figure, due to the nature of the parametric study, the diameter of the bars are not shown, because they are calculated based on a certain reinforcement ratio (tabulated in Table 1) and are not necessarily actual bars that can be found in the industry. The elevation view is depicted only for W-bench. It should be noted that each parameter will be investigated on more walls for a fully understanding of their impacts in a future study by the authors.

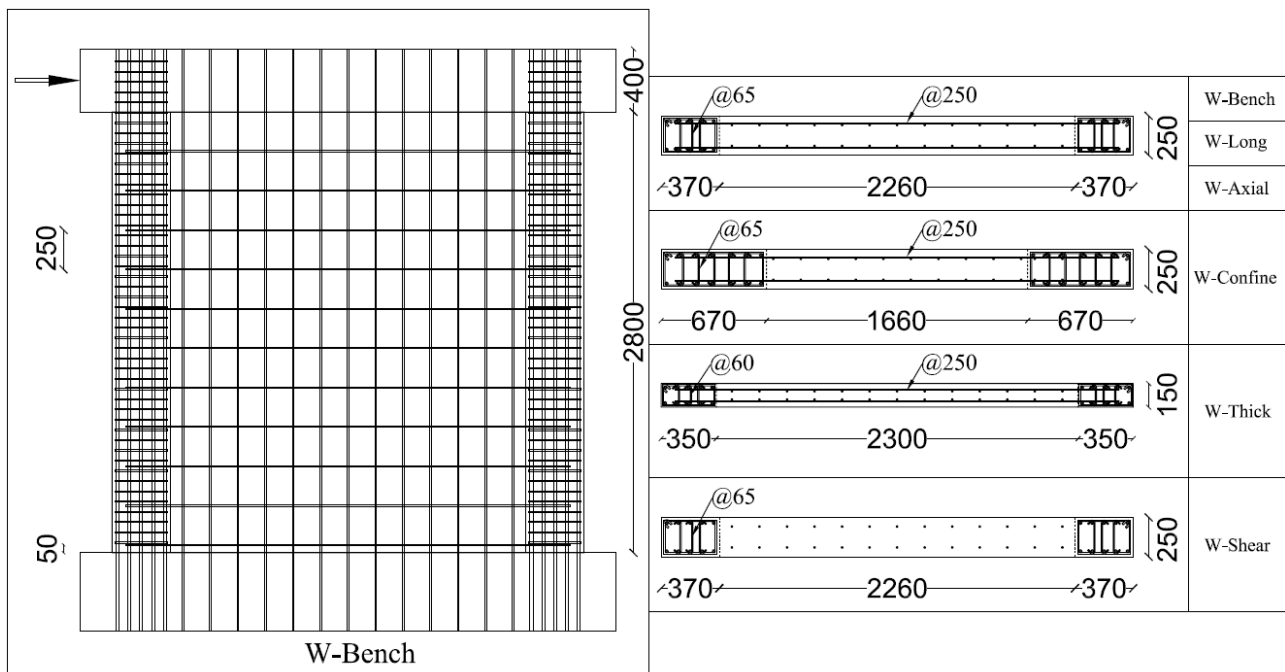


Fig. 4 – Details of walls

The adopted loading protocol for bi-directional loading is shown in Fig. 5; the same loading protocol is previously used by other researchers [10, 14, 15] on walls. However, other types of bi-directional loading pattern such as clover leaf will be investigated in a future study by the authors.

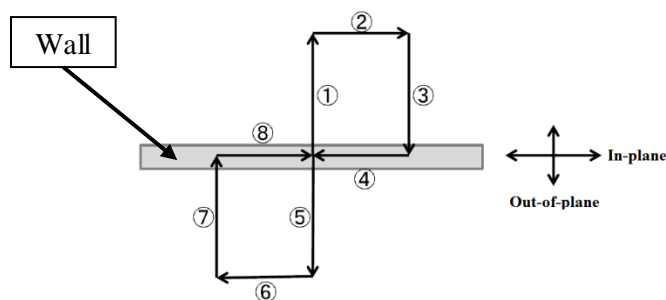


Fig. 5 – Bi-directional loading pattern [10]

3. Finite element modelling

The FE software, DIANA [16], is used to simulate RC walls under uni- and bi-directional loading. Dealing with the complexities involved in nonlinear concrete modelling (compressive and tensile behaviour) in RC structures, availability of material models to incorporate cyclic loading and powerful variety of elements are some of many appealing features of DIANA which led to the selection of this software [11, 17, 18]. A description of the adopted materials and elements is provided below.

3.1 Material Models

3.1.1 Concrete: total strain rotating crack model

Total strain rotating crack model based on the modified compression field theory originally developed by Vecchio et al. [19], is used to model concrete. This model follows a smeared crack approach for the fracture energy [20]. The model proposed by Mander et al. [21] is used to define confined and unconfined concrete. One of the other inputs required for the total strain rotating crack model is the concrete response under uniaxial tensile loading. The uniaxial concrete response under tension is defined following the model proposed by Belarbi and Hsu [22].

3.1.2 Steel reinforcement: Menegotto-Pinto model

The Menegotto-Pinto [23] model which has a bilinear backbone curve and considers Bauschinger effect is used to model steel reinforcements (Fig. 6a). As pointed out by Filippou et al. [24], isotropic hardening can significantly affect the cyclic behaviour of reinforcing bars in RC members. It can have a substantial effect on strain development in bars during crack closure (Fig. 6b). The stress shift to the yield asymptote proposed by Filippou et al. [24] (Fig. 6b) improves the Menegotto-Pinto model in strain prediction of reinforcing bars. It is worth noting that these modifications are implemented in the Menegotto-Pinto model in DIANA [16].

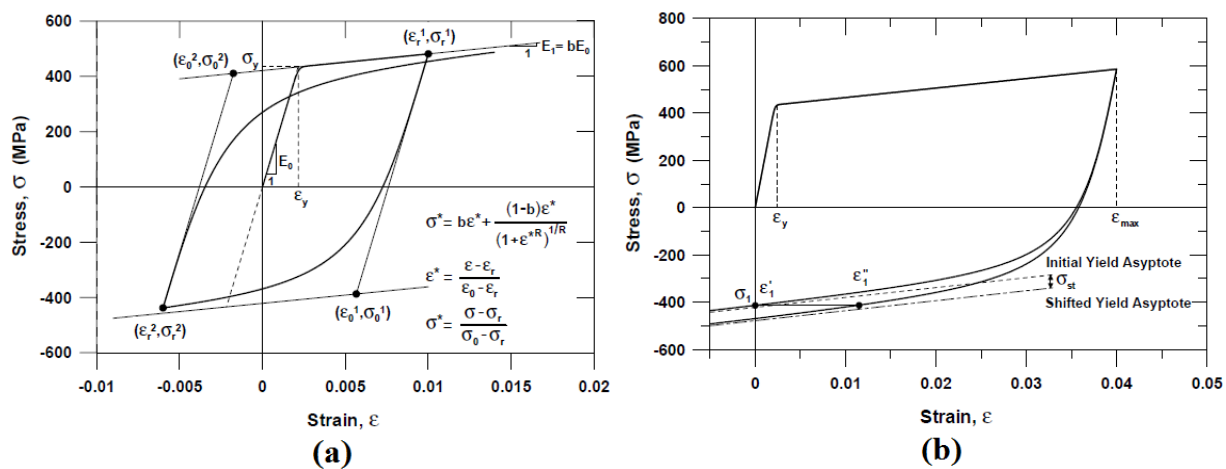


Fig. 6 – Steel reinforcement model (a) Constitutive model [23] (b) Stress shift due to isotropic strain hardening [24]

3.2 Choice of elements

DIANA provides a wide selection of different elements. Solid and shell elements are the two possible options to model walls. Solid elements tend to produce large system of equations; these are usually utilized only when the other elements are either unsuitable or produce inaccurate results. When selecting solid elements increases the computational effort and time required for the analysis without adding significant value to the final outcome, two-dimensional elements (shell) may be used. Thus, curved shell elements (Fig. 7) which proved to be suitable for modelling walls [11, 17] are used for this study. By employing the curved shell elements, location of steel reinforcements (longitudinal and transverse) along the thickness of wall can be defined and different diameter bars may be modelled if necessary (Fig. 10 and 11). This is not possible when using traditional shell elements. In addition, by using curved shell elements the out-of-plane deformations may be accounted for in case of bi-directional loading [11] or to simulate out-of-plane instability [17].

The curved shell elements in DIANA (Fig. 7) are defined based on isoparametric degenerated-solid approach by introducing two shell hypotheses [16] as follows.

Straight-normals: assumes that normals remain straight, but not necessarily normal to the reference surface. Transverse shear deformation is included according to the Mindlin–Reissner theory [25-27].

Zero-normal-stress: assumes that the normal stress component in the normal direction of a lamina basis is forced to zero (i.e. $\sigma_{zz}(\xi, \eta, z) = 0$). The element tangent plane is spanned by a lamina basis which corresponds to a local Cartesian coordinate system (x_l, y_l) defined at each point of the shell with x_l and y_l tangent to the ξ, η plane and z_l perpendicular to it.

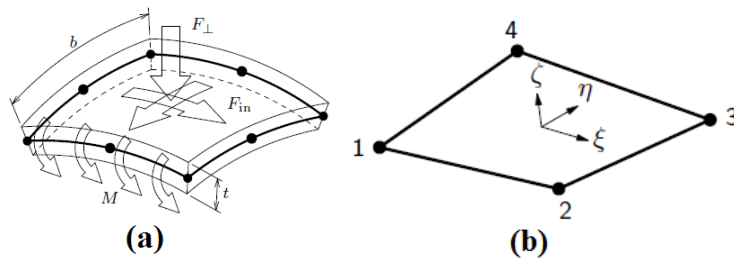


Fig. 7 – Curved shell elements (a) Characteristics and (b) Q20SH - quadrilateral, 4 nodes [16]

Five degrees of freedom are defined in every element node: three translations and two rotations (Fig. 8). The basic variables in the nodes of the curved shell elements are the translations u_X , u_Y and u_Z in the global XYZ directions (Fig. 8a) and the rotations ϕ_x and ϕ_y around the local $+x$ and $+y$ axes in the tangent plane (Fig. 8b).

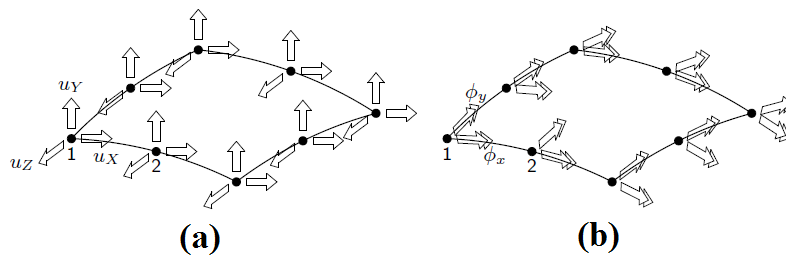


Fig. 8 – Displacements (a) Translations, (b) Rotations [16]

The displacements in the nodes yield the deformations du_X , du_Y and du_Z of an infinitesimal part dX dY (Fig. 9a) and the deformations $d\phi_x$, $d\phi_y$ of an infinitesimal part $d\hat{x}$ $d\hat{y}$ (Fig. 9b). From these deformations, DIANA derives the Green–Lagrange strains in the local $\hat{x}\hat{y}\hat{z}$ axes.

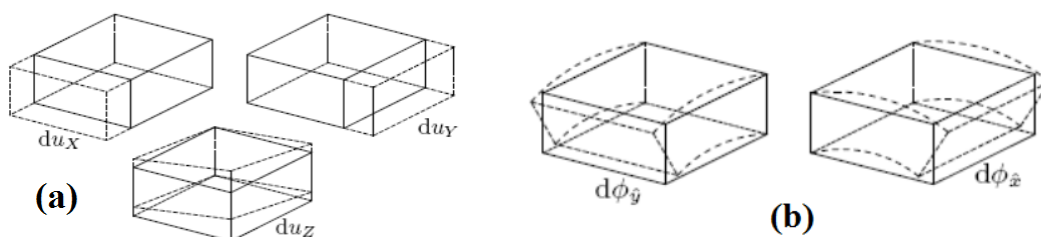


Fig. 9 – Strains (a) Translations, (b) Rotations [16]

Figs. 10 and 11 show the FE models of W-Bench in DIANA. The walls analysed here have cantilever and double-curvature deformation in the in-plane and out-of-plane directions, respectively. As seen in Table 1, the shear span ratio of the wall is 1 and 0.5 in the in-plane and out-of-plane direction, respectively. The double curvature deformation is considered in the out-of-plane direction, simulating the worst case scenario resulted from a moment resisting frame system in the out-of-plane direction. The out-of-plane deformation is introduced using a rigid lever arm as shown in Fig. 11a. The reason of having a double curvature in the out-of-plane direction is to increase the shear demand which can be crucial in case of squat walls.

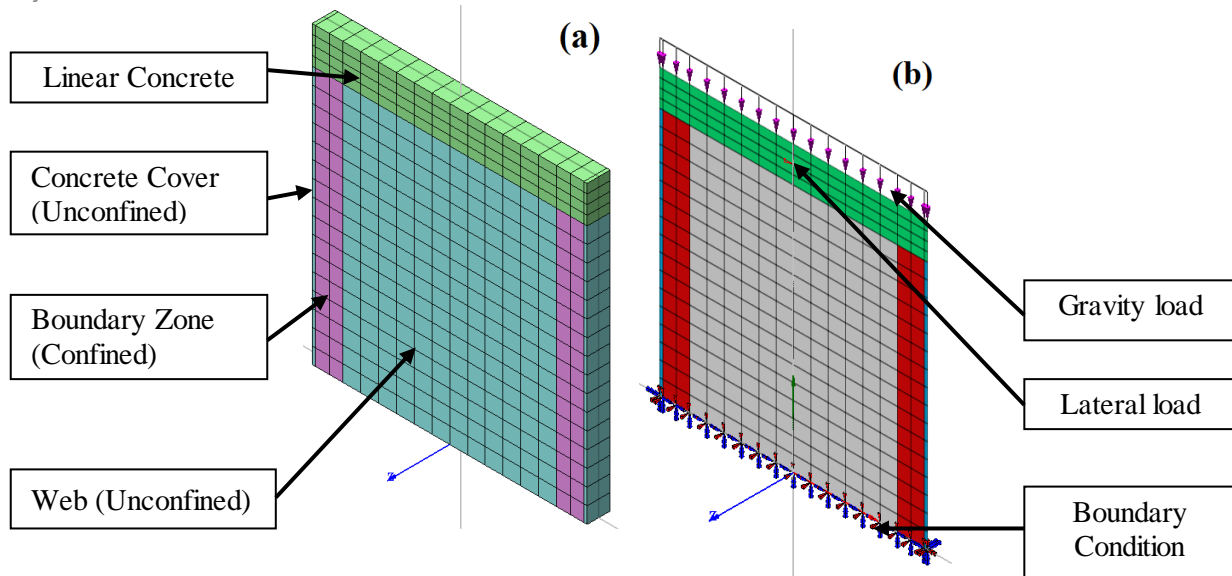


Fig. 10 – Finite Element Model of W-Bench-1D (a) Materials Assignment (b) boundary conditions and loadings

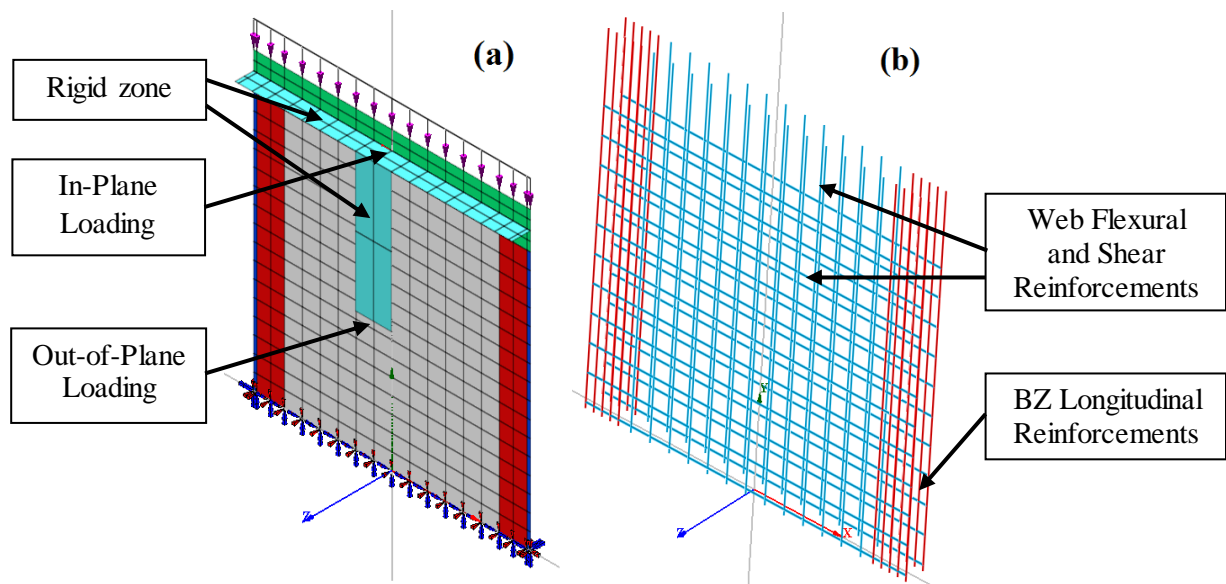


Fig. 11 – Finite Element Model of W-Bench-2D (a) boundary conditions and loadings (b) steel reinforcements

4. Analyses

Table 3 shows the force-displacement curve and failure pattern of each wall. The 1D and 2D suffixes to wall names refer to the uni- and bi-directional loading patterns, respectively. In this table, the red and black circles on the force-displacement curves show the failure point of the walls under uni- and bi-directional loadings, respectively. It should be noted that the failure point is herein assumed when 20% reduction in the strength capacity is observed [5]. Failure modes are shown using the equivalent Von Mises strain contours. Equivalent Von Mises strain is the corresponding equivalent strain at the onset of plastic yielding and beyond calculated using Eq. (1-5) [16]. e_{xx} , e_{yy} and e_{zz} are the deviatoric strains in each direction determined using Eq. (2-4). γ_{ij} is the engineering strain which is defined by Eq. (5). Strain contours shown in Table 3 are at the failure point of each wall. Strain's values are shown on the contours for simplicity.

$$\varepsilon_{eq} = \frac{2}{3} \sqrt{\frac{3(e_{xx}^2 + e_{yy}^2 + e_{zz}^2)}{2} + \frac{3(\gamma_{xy}^2 + \gamma_{yz}^2 + \gamma_{zx}^2)}{4}} \quad (1)$$

$$e_{xx} = \frac{2}{3}\varepsilon_{xx} - \frac{1}{3}\varepsilon_{yy} - \frac{1}{3}\varepsilon_{zz} \quad (2)$$

$$e_{yy} = -\frac{1}{3}\varepsilon_{xx} + \frac{2}{3}\varepsilon_{yy} - \frac{1}{3}\varepsilon_{zz} \quad (3)$$

$$e_{zz} = -\frac{1}{3}\varepsilon_{xx} - \frac{1}{3}\varepsilon_{yy} + \frac{2}{3}\varepsilon_{zz} \quad (4)$$

$$\gamma_{ij} = 2 \times \varepsilon_{ij} \quad (5)$$

Table 3 – Force-displacement curve and failure pattern of each wall

Wall name	Force-displacement curve	Equivalent Von Mises strain - 1D	Equivalent Von Mises strain - 2D
W-Bench			
W-Confine			
W-Thick			
W-Long			

Table 3 Continued – Force-displacement curve and failure pattern of each wall

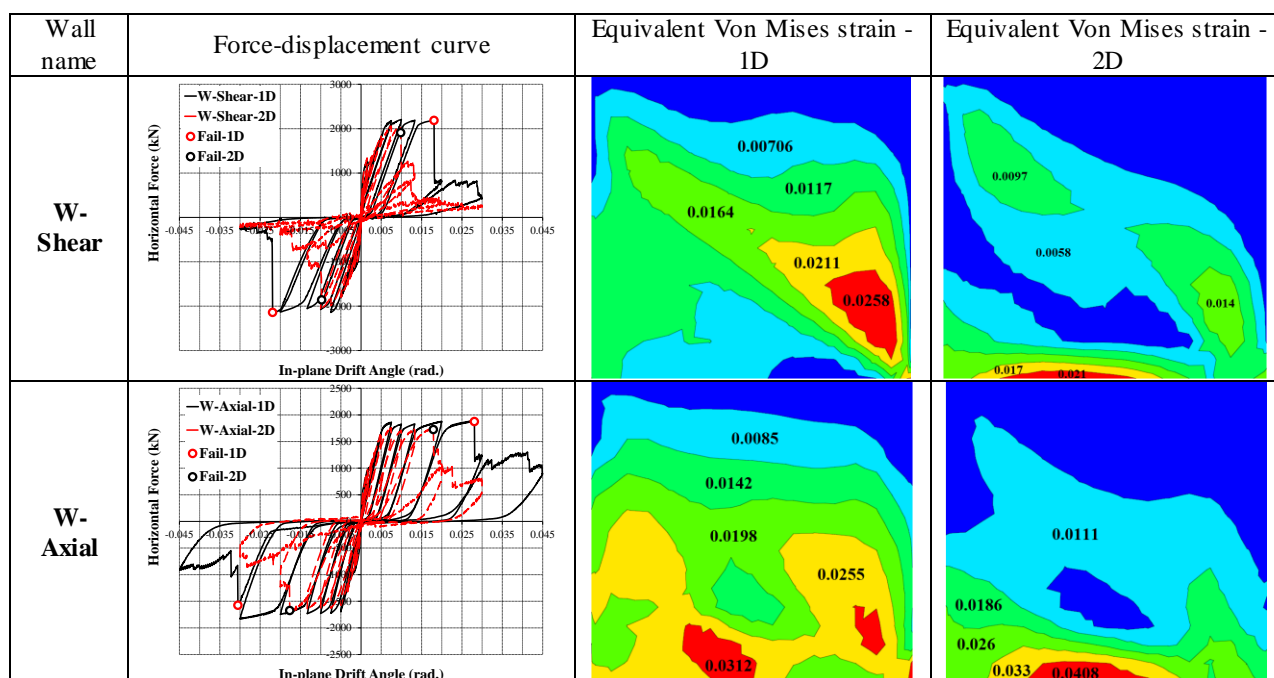


Table 4 shows the ultimate drift, maximum strength capacity and failure mode of each wall. As already mentioned, the ultimate drift ratio is considered when 20% reduction in the strength capacity is observed [5].

Table 4 – Ultimate drift, maximum strength and failure mode of each wall

Wall name	Ultimate drift capacity (+)	Ultimate drift capacity (-)	Maximum strength capacity (kN)	Maximum strength capacity (kN)	Failure mode
W-Bench-1D	0.0218	-0.0221	2282	-2196	Diagonal compression
W-Bench-2D	0.0111	-0.01	2155	-2117	Sliding shear
W-Confine-1D	0.0338	-0.0371	2243	-2185	Diagonal compression
W-Confine-2D	0.0189	-0.0166	2134	-2054	Sliding shear
W-Thick-1D	0.0215	-0.0218	1377	-1323	Diagonal compression
W-Thick-2D	0.0109	-0.0106	1333	-1280	Sliding shear
W-Long-1D	0.0116	-0.0112	2999	-2888	Diagonal tension
W-Long-2D	0.008	-0.0078	2773	-2675	Diagonal tension and Sliding shear
W-Shear-1D	0.0181	-0.0219	2207	-2143	Diagonal tension
W-Shear-2D	0.0098	-0.01	2061	-2053	Diagonal tension and Sliding shear
W-Axial-1D	0.0281	-0.0305	1895	-1834	Diagonal compression
W-Axial-2D	0.0179	-0.0177	1761	-1673	Sliding shear

5. Discussions

5.1 W-Bench

This is the benchmark wall used as a basis for comparing results of the other four walls when the effect of each parameter is investigated. It has a diagonal compression cracking pattern (similar to the one shown in Fig. 2b) when it is under uni-directional loading; starting from the cycle towards 1% up to the failure point. It should be noted that due to the lack of shear reinforcement in the wall, diagonal tension cracking pattern (similar to Fig. 2a) is formed at 0.17% up to 1% drift, but since the shear load was transferred to the rest of the wall after that, this diagonal tension cracking pattern is not resulted in failure. The same statement was also pointed out by Paulay et al. [4]. However, it requires more investigation for fully understanding of this failure pattern. The same wall under bi-directional loading shows a sliding shear failure (similar to the one shown in Fig. 2c), during the unloading of 0.75% drift cycle up to the failure point. Similar result was observed by Kabeyasawa et al. [10]. Although not much difference was observed in the maximum strength (about 6% reduction) and stiffness, a 97% and 121% reduction in the drift capacity was observed in the positive and negative direction, respectively, under bi-directional loading.

5.2 W-Confine

The effect of confinement length is investigated in W-Confine wall with a 50% increase in the confinement length compared to that of W-Bench wall. W-Confine-1D has a diagonal compression cracking pattern starting from the cycle towards 1% up to the failure point. Whereas the same wall shows a sliding shear failure during the unloading of the 0.75% drift cycle up to the failure point under the bi-directional loading. Similar diagonal tension cracking pattern as the one in W-Bench-1D is also formed in W-Confine-1D at 0.17% up to 1% drift, but afterwards the shear load was transferred to the rest of the wall and it is not resulted in failure. Here again, not much difference was observed in the maximum strength (6% reduction) and stiffness, but a 79% and 123% reduction in the drift capacity was observed under bi-directional loading in the positive and negative direction, respectively.

W-Confine shows similar behaviour in comparison to the benchmark wall in terms of the failure mode under both uni- and bi-directional loadings. The main difference is the drift capacity of W-Confine wall has increased by 55-68% and 66-70% under uni- and bi-directional loadings, respectively.

5.3 W-Thick

The thickness of this wall is decreased by 67% to investigate the effect of this parameter on the seismic performance of the wall. A diagonal compression cracking pattern was observed under uni-directional loading, starting from the cycle towards 1% up to the failure point. Similar diagonal tension cracking pattern as the one in W-Bench-1D is also formed in W-Thick-1D at 0.17% up to 1% drift, but afterwards the shear load was transferred to the rest of the wall and it is not resulted in failure. A sliding shear failure was noted in W-Thick-2D during the unloading of the 0.75% drift cycle up to the failure point. Not much difference was observed in the maximum strength (3% reduction) and stiffness, while the drift capacity in the positive and negative directions has 97% and 106% reduction, respectively.

W-Thick has similar behaviour in comparison to the benchmark wall in terms of drift capacity and failure mode under both uni- and bi-directional loadings.

5.4 W-Long

Longitudinal reinforcement ratio of this wall is increased by 50% to investigate the effect of this parameter. W-Long-1D shows a diagonal tension cracking pattern (similar to Fig. 2a), starting from the 0.17% up to the failure point. The main reason of developing diagonal tension failure may be attributed to the high shear stress in this wall resulting from a higher longitudinal reinforcement ratio and also lack of shear reinforcements in the wall. W-Long-2D also shows a diagonal tension failure starting from the 0.17% up to the failure point. However in W-Long-2D, sliding shear is combined with the diagonal tension failure during the cycle towards 0.5% drift cycle up to the end. Not much difference was observed in the maximum strength (8% reduction) and stiffness, while a reduction of 45% and 44% was observed in the drift capacity in positive and negative cycles, respectively.

W-Long has a significant different behaviour compared to the benchmark wall in terms of drift capacity and failure mode under both uni- and bi-directional loadings. The diagonal compression and sliding shear failure in W-Bench-1D and W-Bench-2D, respectively, became diagonal tension failure in W-Long-1D and W-Long-2D. In terms of drift capacity, W-Long-1D shows a significantly less displacement capacity than the benchmark wall (by 87-97%). It also shows a lower displacement capacity compared to that of the benchmark wall under bi-directional loading (by 28-39%).

5.5 W-Shear

For W-Shear, a wall with no shear reinforcement is investigated. As it is expected, the wall shows a diagonal tension failure under uni- and bi-directional loadings, starting from 0.17% up to the failure point. However in W-Shear-2D, sliding shear is combined with the diagonal tension failure during the unloading of the 0.5% drift cycle up to the end. When the wall is under bi-directional loading, not much difference is observed in the maximum strength (7% reduction) and stiffness, while the drift capacity is reduced by 85% and 119% in the positive and negative directions, respectively.

W-Shear shows a different behaviour compared to the benchmark wall in terms of drift capacity and failure mode under both uni- and bi-directional loadings. The diagonal compression and sliding shear failure modes in the benchmark wall under uni- and bi-directional loadings change to a diagonal tension failure in W-Shear-1D and W-Shear-2D. W-Shear shows lower displacement capacity than the benchmark wall by up to 20% and 11% under uni- and bi-directional loadings, respectively.

5.6 W-Axial

Axial load is decreased to zero in this wall to investigate the effect of this parameter on the seismic performance of the wall. W-Axial-1D has a diagonal compression cracking pattern starting from the cycle towards 0.75% up to the failure point. Whereas the same wall shows a sliding shear failure during the cycle towards 0.75% drift up to the failure point under the bi-directional loading. Similar diagonal tension cracking pattern as the one in W-Bench-1D is also formed in W-Axial-1D at 0.17% up to 0.75% drift, but afterwards the shear load was transferred to the rest of the wall and it is not resulted in failure. Here again, not much difference was observed in the maximum strength (8% reduction) and stiffness, but a 57% and 72% reduction in the drift capacity was observed under bi-directional loading in the positive and negative direction, respectively.

W-Axial shows similar behaviour in comparison to the benchmark wall in terms of the failure mode under both uni- and bi-directional loadings. The main difference is that the drift capacity of the wall with zero axial load has increased by 29-38% and 61-77% under uni- and bi-directional loadings, respectively.

6. Conclusions

A numerical parametric study is conducted on few rectangular squat RC walls under uni- and bi-directional loadings. Based on the FE results and the limited analyses conducted here the following conclusions may be drawn.

1. Increasing confinement length may significantly increase the displacement capacity; however, it seems this cannot prevent the sliding shear failure in the wall under bi-directional loading. It is concluded that sufficient confinement length is essential to insure a proper displacement capacity for squat walls.
2. Reducing the thickness does not seem to significantly affect the displacement capacity and failure mode under uni- and bi-directional loadings in the squat walls. Note that reducing the thickness might lead to an out-of-plane instability which is considered an unfavourable failure mode. However in case of W-Thick, out-of-plane instability did not happen under uni- and bi-directional loadings. Further research is necessary for a more comprehensive conclusion.
3. As expected, the amount of longitudinal reinforcement ratio shows a significant impact on the seismic performance of RC walls. It was shown that, increasing this parameter can dramatically decrease the displacement capacity and changes the failure mode to a diagonal tension failure under uni- and bi-directional loadings in comparison to the benchmark. It can be concluded that restricting the flexural

reinforcement ratio can prevent shear modes of failure. More investigation is required for a better understanding of this parameter.

4. Under uni- and bi-directional loadings, decreasing shear reinforcements reduced the displacement capacity and changed the failure mode to diagonal tension failure in comparison to the benchmark. However, this parameter also requires further investigation to fully understand its impacts.
5. Walls with zero and 5% axial load ratios are investigated. It was confirmed that lower axial load ratio increases the displacement capacity. However it does not change the failure mode of the wall dramatically (the dominated failure mode of squat walls is shear). Higher axial load ratio has not been investigated here due to the nature of squat walls.
6. It can be concluded that bi-directional loading can significantly reduce the displacement capacity of squat walls and may change the failure mode in squat walls to a sliding shear failure (in the in-plane direction).
7. Overall, with the limited information resulted from this study, it is shown that longitudinal reinforcement ratio has the highest impact on the seismic performance of squat walls, following by that is the shear reinforcement ratio, confinement length, axial load ratio and thickness. However as it was explained before, more walls will be investigated in a future study by the authors for a fully understanding of the influence of each of these parameter on the bi-directional response of rectangular squat walls.

7. Acknowledgements

Financial support of this research was provided by the SAFER Concrete Research Project funded by the Natural Hazards Research Platform (NHRP), the quake centre and the MBIE Wall project.

8. References

1. Paulay T, Priestley MJN (1992): *seismic design of reinforced concrete and masonry buildings*. John Wiley & Sons, Inc.
2. NIST (2014): *Recommendations for Seismic Design of Reinforced Concrete Wall Buildings Based on Studies of the 2010 Maule, Chile Earthquake*.
3. Elwood K, Pampanin S, Kam WY (2012): *22 February 2011 Christchurch earthquake and implications for the design of concrete structures. The International Symposium on Engineering Lessons Learned from the 2011 Great East Japan Earthquake*. Tokyo, Japan.
4. Paulay T, Priestley MJN, Syngge J (1982): *Ductility in earthquake resisting squat shearwalls*. ACI Journal. **79**(4): p. 257-269.
5. ASCE41-13 (2013): *Seismic Evaluation and Retrofit of Existing Buildings*, American Society of Civil Engineers, Reston, Virginia.
6. Hidalgo P, Ledezma CA, Jordan RM (2002): *Seismic behavior of squat reinforced concrete shear walls*. Earthquake Spectra. **18**(2): p. 287-308.
7. Barda F, Hanson JM, Corley WG (1977): *Shear strength of low-rise walls with boundary elements*. Special Publication. **53**: p. 149-202.
8. Greifenhagen C (2006): *Seismic behavior of lightly reinforced concrete squat shear walls*, ÉCOLE POLYTECHNIQUE FÉDÉRALE DE LAUSANNE.
9. Kuang J, Ho Y (2008): *Seismic behavior and ductility of squat reinforced concrete shear walls with nonseismic detailing*. ACI Structural Journal. **105**(2): p. 225.
10. Kabeyasawa T, Kato S, Sato M, Kabeyasawa T, Fukuyama H, Tani M, Kim Y, Hosokawa Y (2014): *Effects of bi-directional lateral loading on the strength and deformability of reinforced concrete walls with/without boundary columns. The Tenth U.S. National Conference on Earthquake Engineering*.
11. Niroomandi A, Pampanin S, Dhakal RP, Soleymani Ashtiani M (2016): *Finite element analysis of RC rectangular shear walls under bi-directional loading. The New Zealand Society for Earthquake Engineering (NZSEE) Annual Technical Conference*. Christchurch, New Zealand.

12. Krolicki J, Maffei J, Calvi GM (2011): *Shear strength of reinforced concrete walls subjected to cyclic loading*. Journal of Earthquake Engineering. **15**(S1): p. 30-71.
13. NZS3101 (2006): *Code of Practice for the Design of Concrete Structures*, Standards Association of New Zealand.
14. Tatsuya I (1996): *Post-yield behaviours of multi-story reinforced concrete shear walls subjected to bilateral deformations under axial loading*. *The Eleventh World Conference on Earthquake Engineering*.
15. Almeida J, Prodan O, Rosso A, Beyer K (2015): *Tests on Thin Reinforced Concrete Walls Subjected to In-plane and Out-of-plane Cyclic Loading*.
16. DIANA (2015): *DIANA Manual Release 9.6*, TNO DIANA BV: Delft, the Netherlands.
17. Dashti F, Dhakal RP, Pampanin S (2014): *Numerical simulation of shear wall failure mechanisms*. *The New Zealand Society for Earthquake Engineering (NZSEE) Annual Technical Conference*. Auckland, New Zealand.
18. Jünemann R, de la Llera JC, Hube MA, Vásquez J, Chacón M (2016): *Inelastic finite element models to assess earthquake damage of RC wall buildings*. *The New Zealand Society for Earthquake Engineering (NZSEE) Annual Technical Conference*. Christchurch, New Zealand.
19. Vecchio FJ, Collins MP (1986): *The modified compression-field theory for reinforced concrete elements subjected to shear*. ACI J. **83**(2): p. 219-231.
20. Litton RW (1975): *A contribution to the analysis of concrete structures under cyclic loading*. University of California, Berkeley.
21. Mander JB, Priestley MJN, Park R (1988): *Theoretical stress-strain model for confined concrete*. Journal of structural engineering. **114**(8): p. 1804-1826.
22. Belarbi A, Hsu TTC (1994): *Constitutive laws of concrete in tension and reinforcing bars stiffened by concrete*. Structural Journal. **91**(4): p. 465-474.
23. Menegotto M, Pinto PE (1973): *Method of analysis for cyclically loaded reinforced concrete frames including changes in geometry and non-elastic behavior of elements under combined normal forces and bending moment*. IASBE Proceedings.
24. Filippou FC, Popov EP, Bertero VV (1983): *Effects of bond deterioration on hysteretic behavior of reinforced concrete joints*: Earthquake Engineering Research Center, University of California, Berkeley, California.
25. Mindlin RD (1951): *Influence of rotary inertia and shear on flexural motions of isotropic elastic plates*.
26. Reissner E (1945): *The effect of transverse shear deformation on the bending of elastic plates*.
27. Reissner E (1947): *On bending of elastic plates*. Quart. Appl. Math. **5**(1): p. 55-68.